

Local structural changes in KNbO_3 under high pressure

A. I. Frenkel,* F. M. Wang, S. Kelly, R. Ingalls, D. Haskel, and E. A. Stern
Department of Physics, Box 351560, University of Washington, Seattle, Washington 98195

Y. Yacoby

Racah Institute of Physics, Hebrew University, Jerusalem 91904, Israel

(Received 13 May 1997)

The local structure of the perovskite KNbO_3 at 77 and 300 K under high pressure, up to 15.8 GPa, has been investigated using the x-ray-absorption fine-structure (XAFS) technique. It is found that the local-structure symmetry *does not* change even though the average macroscopic crystal symmetry changes several times over this same temperature and pressure range. The existence of different local and macroscopic structures means that the local distortions from the average structure are disordered. Other unexpected results obtained from the XAFS measurements are evidence for a decreasing Nb-Nb displacement correlation length and a destabilization of the oxygen octahedra with increasing pressure. [S0163-1829(97)08241-6]

I. INTRODUCTION

It has been recently established that temperature-driven structural phase transitions in several perovskite ferroelectric (PbTiO_3 ,¹ KNbO_3 ,² and $\text{KTa}_x\text{Nb}_{1-x}\text{O}_3$,³) and antiferrodistortive crystals⁴ ($\text{K}_{1-x}\text{Na}_x\text{TaO}_3$), previously believed to be purely displacive, have a significant component of order-disorder. The local structural displacements present in the lower temperature phase persist in the higher temperature phase far above the phase transition temperature. The average and local structural distortions can be separately measured using diffraction techniques and x-ray-absorption fine structure (XAFS), respectively. For example, neutron-diffraction measurements⁵ in KNbO_3 show that the Nb atoms occupy the body-center positions in the cubic phase and are displaced in the [100], [110], and [111] directions in the tetragonal, orthorhombic, and rhombohedral phases, respectively. On the other hand, XAFS measurements, on the same material, show that the Nb atoms are displaced in all phases including the cubic phase in the [111]-type directions.² However, the sense of one or more components of these displacements may be disordered. For example, in the orthorhombic phase the [110] component of the displacements has a non-zero average. However, the [001] component is disordered so that on the average polarization is in the [110] direction. This indicates that the structural phase transition in KNbO_3 has an important element of order-disorder. Comes *et al.*,⁶ suggested this model on the basis of diffuse x-ray scattering experiments. However, these experiments could also be interpreted in a way consistent with a displacive model. Similar effects were observed in other systems as well.

Recently, Girshberg and Yacoby⁷ presented a model of ferroelectrics based on the existence of both a soft mode and spontaneous local off-center ion displacements, and the interaction between the two. Their model accounts quantitatively for both displacive and order-disorder-like properties. For KNbO_3 , for example, their model explains why its Curie-Weiss constant (2.8×10^5 K) is as large as the constant predicted for purely displacive-type crystals and at the same time its soft mode does not vanish at T_c but extrap-

lates to zero at a temperature hundreds of degrees below T_c .

While the effect of temperature on the average and local structure of perovskites has been studied rather extensively, the effect of pressure has not received sufficient attention. It is well known that hydrostatic pressure affects the structural phase transition temperatures of perovskite crystals. The question is how it affects the local structure. In this paper we report the effect of pressure on the local structure of KNbO_3 .

At ambient pressure KNbO_3 undergoes several structural phase transitions from cubic to tetragonal at 708 K and then to orthorhombic and rhombohedral at 498 and 263 K, respectively. Recent birefringence and Raman-scattering experiments by Gourdain *et al.*⁸ suggest that the ferroelectric-paraelectric transition in KNbO_3 takes place at 9–10 GPa and room temperature. The authors describe the structure of the paraelectric phase as cubic and the phase transition as weakly first order. They observed, however, first-order Raman scattering in the paraelectric phase. Such scattering is symmetry forbidden in the cubic structure and is attributed by the authors to the dynamic disorder of Nb atoms which breaks the crystal inversion symmetry. Shen *et al.*⁹ also studied KNbO_3 under pressure by Raman spectroscopy. They, however, report “three new crystalline phases and an amorphous phase” in the pressure range from 0 to 20 GPa. According to the authors, the displacive phase transitions occur at 2, 6, 9, and 15 GPa, respectively. These two quite different results obtained for the same material using the same method emphasize the need for more detailed structural information.

The characteristic time scale of the XAFS experiment (10^{-15} s) is much shorter than the estimated relaxation time of possible Nb ion dynamic disorder. Thus XAFS can measure both types of distortions (dynamic or static) with equal facility. If the relaxation time of dynamically disordered ions is shorter than the characteristic time of Raman-scattering experiments, 10^{-10} – 10^{-11} s, Raman spectroscopy will provide information on the average rather than the instantaneous structure, while XAFS in this case will still provide an instantaneous “snapshot” of the locally distorted structure. However, XAFS alone cannot determine whether the disor-

der present is dynamic, i. e., the atoms hop among the different equivalent off-center positions, or static, i. e., the structure has static local distortions.

The present work obtained detailed local structural information on KNbO_3 at both room and liquid-nitrogen temperatures and pressures up to 15.8 and 10.2 GPa, respectively. The pressure effect on the distances between Nb and its near neighbors, and their corresponding mean-square relative displacements σ^2 at 77 and 300 K were measured. At both temperatures and all the pressures studied, the local structure was obtained to be rhombohedral thus supporting the existence of an important element of order-disorder in the pressure-induced phase transitions similar to the temperature-induced one.

Sample preparation and XAFS measurements under pressure are described in Sec. II. Details of the data analysis are described in Sec. III. The modeling procedure is developed in Sec. IV. The results and discussion are presented in Sec. V. Summary and conclusions are given in Sec. VI.

II. EXPERIMENT

High pressure was achieved by means of a pressure cell¹⁰ using boron carbide anvils with a 1.5 mm tip diameter. Diamond anvils generally produce Bragg glitches which spoil the high-quality XAFS necessary for the precise structural information required here. The anvils were driven with hydraulic oil pressure at room temperature and with helium gas at liquid-nitrogen temperature. The KNbO_3 and Ag powders were obtained from Cerac and Alfa Aesar, respectively. The sample and the Ag pressure calibrant both had particle sizes, x , well below the value corresponding to $\Delta\mu x = 1$, thus avoiding “thickness effects”¹¹ in the transmission XAFS experiment. The powders were mixed with vacuum grease and loaded into a 0.4 mm diameter hole in a 0.25 mm thick Inconel gasket. The incident x-ray beam passed through a confining iris of 0.3 mm diameter to ensure that the same beam passes through the incident beam detector, the sample and the signal detector. The XAFS measurements were performed at the Stanford Synchrotron Radiation Laboratory, beam line IV-3, using a Si (220) double-crystal monochromator. In order to eliminate higher harmonics, the crystals were detuned by 10% for the Nb K -edge measurements. No detuning was necessary for the Ag K -edge measurements.

III. DATA ANALYSIS

The data were processed and analyzed using the UWXAFS data analysis package developed at the University of Washington, Seattle.¹² Some aspects of the analysis were checked with an independent analysis program developed at the Hebrew University of Jerusalem which gave the same results within the error brackets. The normalized XAFS spectra were obtained by subtracting the background $\mu_0(k)$ from the measured absorption coefficient $\mu(k)$ using the AUTOBK method¹³ and were normalized by the edge jump $\Delta\mu_0(0)$:

$$\chi(k) = \frac{\mu(k) - \mu_0(k)}{\Delta\mu_0(0)}. \quad (1)$$

Here k is the photoelectron wave number given by $k = \sqrt{2m(E - E_0)/\hbar^2}$, where m is the electron mass, E is the

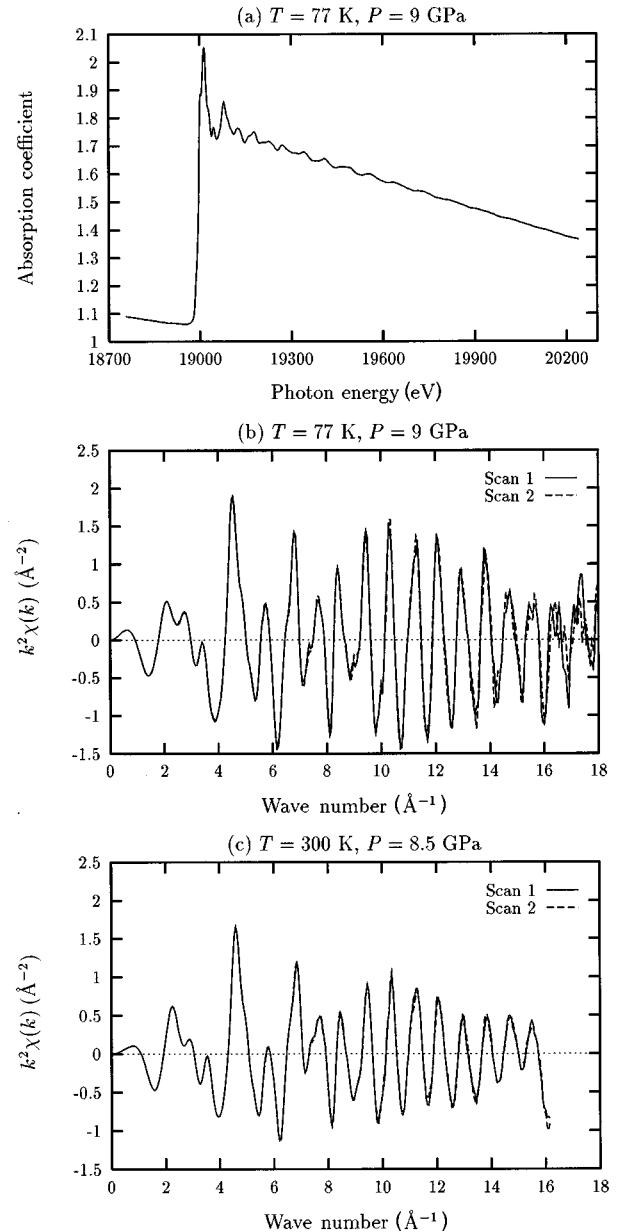


FIG. 1. (a) The measured absorption coefficient μx at 77 K, 9 GPa. k^2 -weighted $\chi(k)$ for two scans measured at (b) 77 K, 9 GPa and (c) 300 K, 8.5 GPa.

x-ray photon energy, and E_0 is the K -edge energy. A typical Nb K -edge spectrum of KNbO_3 is shown in Fig. 1(a).

For the purpose of background removal the energy reference was taken at the middle of the edge jump. The r range for minimizing the signal below the first shell was $r < 1.2 \text{ \AA}$ for KNbO_3 and $r < 1.7 \text{ \AA}$ for the Ag calibrant. The resulting k^2 -weighted $\chi(k)$ at 77 and 300 K at similar pressures (9.0 and 8.5 GPa, respectively) are shown in Figs. 1(b) and 1(c). The spectra of two consecutive measurements at each pressure are presented showing that the statistical noise in the data is relatively low.

The XAFS signal is a sum of paths including both single-scattering (SS) and multiple-scattering (MS) contributions:¹⁴ $\chi(k) = \sum_{\Gamma} \chi_{\Gamma}(k)$. The contribution of each path can be expressed in the form:

$$\chi_I(k) = \frac{S_0^2 N}{kr^2} f(k) e^{-2k^2 \sigma^2} \sin(2kr + \delta(k)) e^{-2r/\lambda(k)}, \quad (2)$$

where S_0^2 is the passive electron reduction factor,¹⁴ N is the coordination number of the shells of neighboring atoms in case of the SS paths, or the number of equivalent scattering configurations, including time reversed in the case of the MS paths, r is half the total scattering path length, σ^2 is the corresponding mean-square relative displacement, $f(k)$ and $\delta(k)$ are the effective scattering amplitude and phase shift, respectively, and $\lambda(k)$ is the mean free path.

$f(k)$, $\delta(k)$, and $\lambda(k)$ were calculated for the reference cubic and rhombohedral structures of KNbO_3 (see Sec. IV) using the FEFF6 code of Zabinsky *et al.*¹⁵ The unit-cell distortion parameters defined in the next section, the σ^2 and the muffin-tin energy reference corrections ΔE_0 were determined from the nonlinear least-squares fit of theory to data. Both data and theory were multiplied by either k , k^2 or k^3 and by a Hanning window function with margins of 2 \AA^{-1} and then Fourier transformed into r space where the fits were performed. The fitting ranges in k and r spaces and the weighting factors are discussed in detail in Sec. V.

Fits to the Ag calibrant data were performed to determine the actual pressure in the sample cell at both 77 and 300 K. These fits provided the nearest-neighbor distance for each pressure. The actual pressure points for the room-temperature data were determined by comparing the measured compression of the interatomic distances with those provided in the compressibility tables.¹⁶ At room temperature the pressure points were: 1.4, 5.3, 8.5, 11.6, and 15.8 GPa (with 0.4 GPa uncertainty). The pressure points at liquid-nitrogen temperature were determined in the same way after correcting for $\sim 9\%$ increase in the bulk modulus of Ag at 77 K relative to 300 K.¹⁷ The resulting pressure points at 77 K were ambient, 3.4, 4.3, 9, and 10.2 GPa (with 0.4 GPa uncertainty).

IV. MODEL OF LOCAL DISTORTIONS

As shown by previous XAFS measurements of KNbO_3 at ambient pressure at various temperatures² and $\text{KNb}_{0.87}\text{Ta}_{0.13}\text{O}_3$ at ambient temperature under pressure,¹⁸ the local structure around the Nb atoms preserves its low-temperature rhombohedral distortion, even above the rhombohedral-orthorhombic phase transition temperature. The macroscopic orthorhombic distortion is, therefore, obtained by averaging over the disordered rhombohedral local distortions. We attempted to fit our data at ambient pressure assuming the orthorhombic structure model,⁵ but the fit quality was much worse than that obtained using the rhombohedral model. This confirms previously obtained results.^{2,18} These results, together with other studies of the local structure of other perovskites which show that the high-temperature local structure remains similar to the structure of the lowest-temperature phase,^{1,3,4,19} support the use of the rhombohedral model as the basis of our analysis.

The atomic positions in the rhombohedral $R3m$ phase are⁵

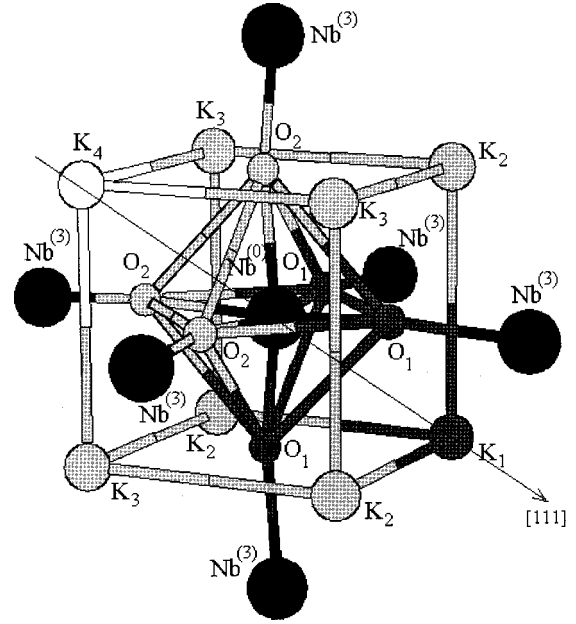


FIG. 2. Rhombohedral structure of KNbO_3 .

$$\text{K at } \Delta(\text{K}), \Delta(\text{K}), \Delta(\text{K}),$$

$$\text{Nb at } \frac{1}{2}, \frac{1}{2}, \frac{1}{2},$$

$$\text{O at } \frac{1}{2} + \Delta_x(\text{O}), \frac{1}{2} + \Delta_x(\text{O}), \Delta_z(\text{O}). \quad (3)$$

At 230 K, the lattice parameter was found to be $a = 4.016 \text{ \AA}$, the rhombohedral angle $\alpha = 89.83^\circ$, $\Delta_x(\text{O}) = 0.0295(5)$, $\Delta_z(\text{O}) = 0.0308(7)$, and $\Delta(\text{K}) = 0.0112(25)$.

Figure 2 shows three nearest coordination shells, $\text{O}^{(1)}$, $\text{K}^{(2)}$, and $\text{Nb}^{(3)}$, around the central $\text{Nb}^{(0)}$ atom. The superscript denotes the shell number. The oxygen octahedron splits into two subshells, denoted O_1 and O_2 with three oxygen atoms each. The potassium cube splits into four subshells with 1, 3, 3, and 1 K atoms, denoted K_1 , K_2 , K_3 , and K_4 , respectively. Not shown is the fourth-nearest coordination shell of 24 oxygen atoms from neighboring octahedra. They are also rhombohedrally displaced relative to the $\text{Nb}^{(0)}$ probe forming four subshells with six oxygen atoms each. Finally, the fifth shell consists of 12 niobium atoms. Assuming all Nb atoms are displaced in the same direction this shell does not split.

FEFF6 calculations show that the important scattering configurations with path lengths shorter than or equal to twice the $\text{Nb}^{(0)}\text{-Nb}^{(5)}$ distance are single-scattering (SS) paths to $\text{O}^{(1)}$, $\text{K}^{(2)}$, $\text{Nb}^{(3)}$, $\text{O}^{(4)}$, and $\text{Nb}^{(5)}$ neighbors, collinear double-scattering (DS), and triple-scattering (TS) paths $\text{Nb}^{(0)}\text{-O}^{(1)}\text{-Nb}^{(3)}\text{-O}^{(1)}\text{-Nb}^{(0)}$, and collinear TS paths $\text{Nb}^{(0)}\text{-O}_1\text{-Nb}^{(0)}\text{-O}_2\text{-Nb}^{(0)}$.

If all the structural coordinates were varied independently, the total number of variables (N_{var}) would exceed the number of independent data points N_{idp} where $N_{\text{idp}} = 2\Delta k \Delta r / \pi + 2$ and Δk and Δr are the k and r ranges of the data used in the analysis.²⁰

The difference between $\Delta_x(\text{O})$ and $\Delta_z(\text{O})$ and the deviation of α from 90° are too small to affect the XAFS results.

Thus in our analysis we have used two independent structural distortion parameters: $\Delta(\text{O})$ and $\Delta(\text{K})$. We assumed that under pressure the distortion parameters may vary within the ranges: $0 < \Delta(\text{O}) < \Delta^{\text{max}}(\text{O}) = 0.034$ and $0 < \Delta(\text{K}) < \Delta^{\text{max}}(\text{K}) = 0.012$.

Any function $\Psi(R_{ij})$ in the XAFS equation [Eq. (2)] which depends on the distances R_{ij} between pairs of atoms in the rhombohedrally distorted structure (e.g., backscattering amplitude, phase shift or the distance itself) is, therefore, a function of these two variables, and in the linear approximation can be approximated as

$$\Psi(\Delta(\text{O}), \Delta(\text{K})) \approx \Psi^{\text{cubic}} + \frac{\partial \Psi}{\partial \Delta(\text{O})} \Delta(\text{O}) + \frac{\partial \Psi}{\partial \Delta(\text{K})} \Delta(\text{K}), \quad (4)$$

where $\Psi^{\text{cubic}} = \Psi(0,0)$ is the function in the cubic model. An important exception from the linear behavior is the rapidly oscillating function $\Psi(R_{ij}) = \sin(2kR_{ij} + \delta(k))$ [Eq. (2)]. This function, however, can be calculated exactly for each value of R_{ij} , which is, in turn, approximated using Eq. (4).

Using Eq. (4), and allowing for the isotropic contraction of the unit cell with pressure P by a factor $\epsilon(P) = a(P)/a_0$, where a_0 is the lattice constant in the initial cubic model, the interatomic distances between Nb and its nearest neighbors (Fig. 2) can be calculated at any pressure in the following way:

$$\begin{aligned} R_{\text{Nb-O}_i}^{(1)} &= \epsilon R_{\text{Nb-O}}^{\text{cubic}(1)} + \frac{\partial R_{\text{Nb-O}_i}^{(1)}}{\partial \Delta(\text{O})} \Delta(\text{O}); \quad i = 1, 2, \\ R_{\text{Nb-K}_i}^{(2)} &= \epsilon R_{\text{Nb-K}}^{\text{cubic}(2)} + \frac{\partial R_{\text{Nb-K}_i}^{(2)}}{\partial \Delta(\text{K})} \Delta(\text{K}); \quad i = 1, 2, 3, 4, \\ R_{\text{Nb-Nb}}^{(3)} &= \epsilon R_{\text{Nb-Nb}}^{\text{cubic}(3)}, \\ R_{\text{Nb-O}_i}^{(4)} &= \epsilon R_{\text{Nb-O}}^{\text{cubic}(4)} + \frac{\partial R_{\text{Nb-O}_i}^{(4)}}{\partial \Delta(\text{O})} \Delta(\text{O}); \quad i = 1, 2, 3, 4. \end{aligned} \quad (5)$$

The partial derivatives in Eq. (5) were obtained by applying distortions $\Delta^{\text{max}}(\text{O})$ and $\Delta^{\text{max}}(\text{K})$ to the cubic unit cell, and calculating the increment in interatomic distances resulting from each distortion. We checked how good these linear approximations are by comparing the exact distances to those calculated from Eqs. (5) for $\Delta(\text{O}) = 0.017$ and $\Delta(\text{K}) = 0.006$. The deviations are less than 0.004 \AA .

Scattering amplitudes $f(k)$, phase shifts $\delta(k)$ and mean free paths $\lambda(k)$ of the SS paths are not very sensitive to the small changes in the path lengths (less than 0.4 \AA).¹⁵ Thus these functions were calculated for the initial cubic structure model and were not changed in the fit process. On the other hand, $f(k)$ of the collinear multiple-scattering (DS and TS) paths $\text{Nb}^{(0)}\text{-O}^{(1)}\text{-Nb}^{(3)}\text{-O}^{(1)}\text{-Nb}^{(0)}$ and $\text{Nb}^{(0)}\text{-O}_1\text{-Nb}^{(0)}\text{-O}_2\text{-Nb}^{(0)}$, are sensitive to the deviations from collinearity.^{21,22} For small buckling angles they can be approximated with the quadratic term in the Taylor expansion:²³

$$f(k, \Delta(\text{O})) = f^{\text{cubic}}(k, 0) + \frac{1}{2} \frac{\partial^2 f}{\partial \Delta^2(\text{O})} \Delta^2(\text{O}), \quad (6)$$

where the first term in the right part is the scattering amplitude in the undistorted cubic structure. Using the value for $\Delta^{\text{max}}(\text{O})$, the second derivative of Eq. (6) can be evaluated as

$$\frac{\partial^2 f}{\partial \Delta^2(\text{O})} = \frac{2}{(\Delta^{\text{max}}(\text{O}))^2} [f(k, \Delta^{\text{max}}(\text{O})) - f^{\text{cubic}}(k, 0)]. \quad (7)$$

$f(k, \Delta^{\text{max}}(\text{O}))$ and $f^{\text{cubic}}(k, 0)$ were calculated using FEFF6.

Equations (5) and (6) were used to constrain all the interatomic distances and scattering amplitudes of multiple-scattering paths to vary in accordance with just three variables: $\Delta(\text{O})$, $\Delta(\text{K})$, and ϵ .

The σ^2 of different neighboring shells were varied independently; the σ^2 of the subshells were set equal to the shell σ^2 , except for the first-nearest-neighbor (1NN): we found that the quality of fit is better if $\sigma_{\text{Nb-O}_1}^2$ and $\sigma_{\text{Nb-O}_2}^2$ are allowed to be different. Other constraints were applied to relate the σ^2 of the SS path $\text{Nb}^{(0)}\text{-Nb}^{(3)}$ to those of collinear DS and TS paths from $\text{Nb}^{(0)}$ through $\text{O}^{(1)}$ to the next $\text{Nb}^{(3)}$ in a row: $\sigma_{\text{SS}}^2 = \sigma_{\text{DS}}^2 = \sigma_{\text{TS}}^2$. The σ^2 of the TS path $\text{Nb}^{(0)}\text{-O}_1\text{-Nb}^{(0)}\text{-O}_2\text{-Nb}^{(0)}$ was constrained to be equal to $\sigma_{\text{Nb-O}_1}^2 + \sigma_{\text{Nb-O}_2}^2$. These constraints are good approximations for almost collinear bonds,²⁴ which is the case here.

S_0^2 was determined from the fit to the ambient pressure room-temperature data (0.90 ± 0.05) and was fixed for the rest of the pressure points. To break the correlation between S_0^2 and σ^2 , we used a method suggested by Koningsberger.²⁵ For each weighting factor k , k^2 , and k^3 , used in the Fourier transform, we varied S_0^2 from 0.7 to 1.0 (the typical range of reasonable values for S_0^2) with a 0.05 increment and obtained σ^2 for the first 1NN bonds from the best fit. σ^2 was then plotted as a function of S_0^2 for each weighting factor. The three curves intersect at almost the same point providing the values of S_0^2 and σ^2 .

FEFF6 assumes that the material can be approximated by an array of neutral atoms which neglects the electrostatic potentials induced by charge transfer. To correct for this approximation, it is necessary to introduce different energy reference values E_0 for different paths. As shown by Haskell *et al.*²⁶ for the perovskite BaZrO_3 , it is sufficient to assign different ΔE_0 shifts to different SS paths and to relate the ΔE_0 of the MS paths to those of SS paths in accordance with the number of times the photoelectron is scattered by each scattering atom.

These constraints reduce the number of variables dramatically: the total number of fit parameters N_{var} used in our fits was 12, thus, much fewer than the number of relevant independent experimental points $N_{\text{idp}} = 22 - 24$, depending on the data range in k and r spaces.

V. FIT RESULTS AND DISCUSSION

Fourier-transform amplitudes of the fits between the k^2 -weighted theory and data at 77 K at ambient pressure and 10.2 GPa are shown in Fig. 3. Fits to the room-temperature data are shown in Fig. 4 (ambient pressure) and Fig. 5 (15.8 GPa).

Visual inspection of Figs. 3–5 shows that the intensity of structures at distances below about 4 \AA grows with pressure relative to the structures above it at both temperatures. One

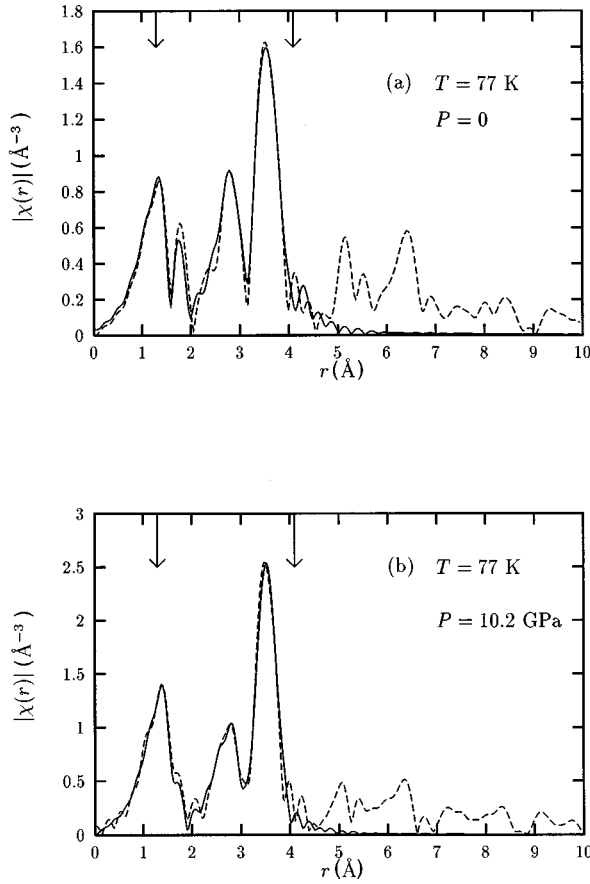


FIG. 3. Fits of theory (solid) to k^2 -weighted Fourier-transformed data (dash) at 77 K. (a) Ambient pressure, (b) 10.2 GPa.

normally expects a decrease in σ^2 with the increasing pressure. This explains the increase of intensity of the first few shells. The different behavior of the O⁽⁴⁾ and Nb⁽⁵⁾ shell XAFS contributions is, therefore, particularly interesting.

Special care was taken to extract the fourth oxygen and the fifth Nb shell information. Oxygen octahedra are reported to behave anomalously with temperature [in the case of pure KNbO₃ (Ref. 5)] and pressure [in the case of KNb_{0.87}Ta_{0.13}O₃ (Ref. 18)], and thus precise local structural information is particularly valuable since the 4NN and 1NN oxygen atoms belong to different octahedra. The anomaly, in the case of pure KNbO₃ is revealed in the large anisotropy of the mean-square displacements of the oxygen atoms observed in neutron-diffraction experiments.⁵ In the case of KNb_{0.87}Ta_{0.13}O₃ the σ^2 of Nb-O⁽⁴⁾ were found to increase with pressure, in contrast to expectations.

The different change in intensity of the first three shells and the 4NN oxygen and 5NN niobium shells complicates the simultaneous fitting of these shells. We were able to analyze the contributions of the higher r shells separately from the lower r shells, as described below. In contrast to Nb, the amplitude function of oxygen is large only at relatively small k . Thus to observe the 4NN oxygen contribution it is better to use k^1 weighting. We therefore analyzed the data in two steps. First, we used k^2 weighting and the entire k range (from 2 to 15 \AA^{-1}) to fit the entire r range (from 1.3 to 4.1 \AA) at once, since the parameters of different paths are coupled through Eqs. (5) and (6). As a result, we found the

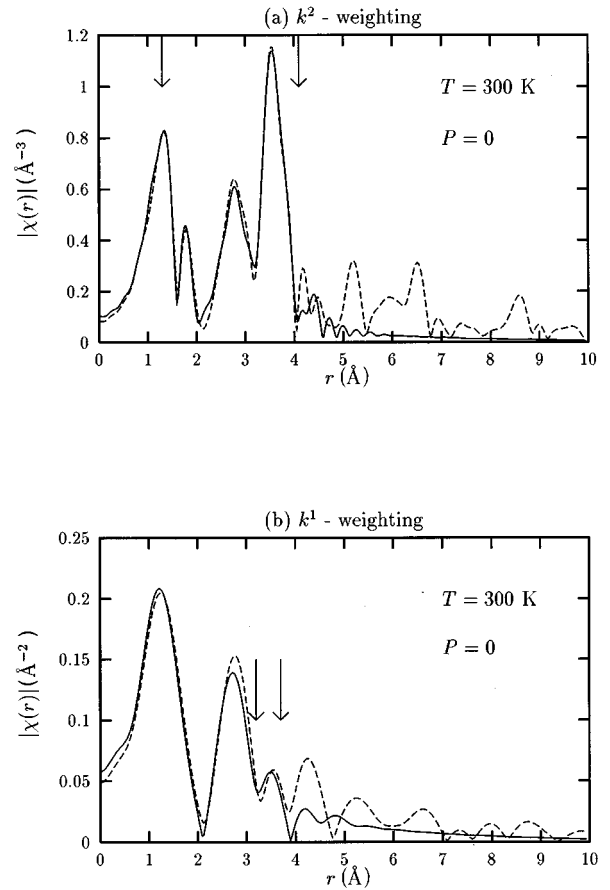


FIG. 4. Fits of theory (solid) to data (dash) at $T=300$ K and ambient pressure. Fitting range is indicated by arrows. Fourier-transform parameters: (a) k range: $2 \text{\AA}^{-1} < k < 14 \text{\AA}^{-1}$, weighting factor: k^2 , (b) k range: $2 \text{\AA}^{-1} < k < 7 \text{\AA}^{-1}$, weighting factor: k^1 .

structural parameters and energy reference shifts with high precision for all the paths except those of the 4NN. Then, in a second step, we fixed the variables of all paths except 4NN to be equal to the above best-fit results, and fit the σ^2 and ΔE_0 for the 4NN paths using k^1 weighting and a much smaller k range: $2 < k < 7 \text{\AA}^{-1}$ and r range: $3.2 < r < 3.7 \text{\AA}$, where the 4NN oxygens contribute most. The data and fit in r space demonstrating this two-step fitting procedure are shown in Figs. 4 and 5 for the room-temperature measurements at ambient and 15.8 GPa pressure, respectively. In this manner, we obtained relatively accurate values for the 4NN oxygen shell σ^2 .

Nb⁽⁰⁾-Nb⁽⁵⁾ pairs are oriented in a [110] direction in the cubic structure. Since there are no intervening atoms between Nb⁽⁰⁾ and Nb⁽⁵⁾ (Fig. 2), the contributions of the SS Nb⁽⁰⁾-Nb⁽⁵⁾ paths dominate this r range. Some of the noncolinear MS paths include oxygens, and therefore, mainly contribute to the XAFS in a lower k region than the Nb⁽⁰⁾-Nb⁽⁵⁾ paths. To minimize the interference with these MS paths the low limit of the k fitting range was set to 5 \AA^{-1} . The Nb⁽⁵⁾ shell was analyzed within the r range between 4.8 and 5.5 \AA . We used a k^3 weighting factor and a k range of 5–14 \AA^{-1} . The number of independent data points was 5. The XAFS contributions of these shells was calculated using FEFF6 assuming the rhombohedral distortions and the unit-cell parameters found from the previous fits in the $1.3 < r < 4.1 \text{\AA}$

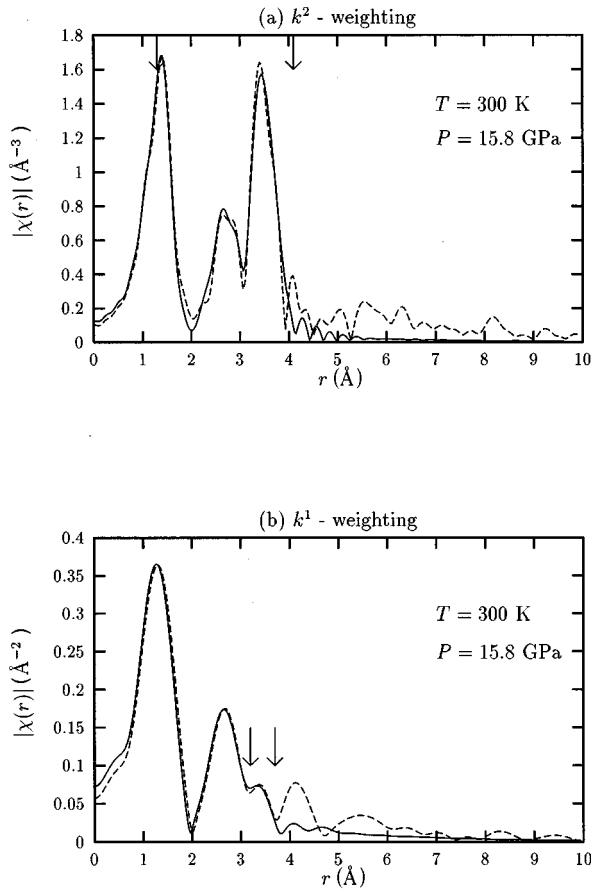


FIG. 5. Fits of theory (solid) to data (dash) at $T=300$ K and $P=15.8$ GPa. Fitting range is indicated by arrows. Fourier transform parameters: (a) k range: $2 \text{ \AA}^{-1} < k < 14 \text{ \AA}^{-1}$, weighting factor: k^2 , (b) k range: $2 \text{ \AA}^{-1} < k < 7 \text{ \AA}^{-1}$, weighting factor: k^1 .

range. The only fitting parameters were the σ^2 and the energy reference correction. Fit results are shown in Figs. 6 and 7 for two pressures, ambient and the highest pressure achieved, at 77 and 300 K, respectively.

Numerical results for $\Delta(\text{O})$, the lattice parameter a and the Nb off-center displacement d relative to the oxygen octahedra are tabulated in Tables I and II at all pressures measured at 77 and 300 K, respectively. The values of $\Delta(\text{K})$ and the $\text{Nb}^{(0)\text{-K}^{(2)}} \sigma^2$ are comparable to the uncertainties at all pressures and temperatures, and are therefore omitted.

The pressure dependence of the Nb off-center displacements are shown in Fig. 8. The ambient pressure displacements at both 77 and 300 K (i.e., below and above the rhombohedral—orthorhombic phase transition temperature) are in good agreement with the 0.218 \AA displacement mea-

TABLE I. Atomic coordinates $\Delta(\text{O})$, unit cell size a , Nb off-center displacement d at 77 K and different pressures.

P (GPa)	$\Delta(\text{O})$	a , \AA	d , \AA
0	0.0261(11)	4.034(8)	0.183(5)
3.4(4)	0.0232(12)	3.990(6)	0.161(5)
4.3(4)	0.0233(13)	3.990(6)	0.162(5)
9.0(4)	0.0180(16)	3.947(7)	0.123(7)
10.2(4)	0.0177(12)	3.949(6)	0.121(5)

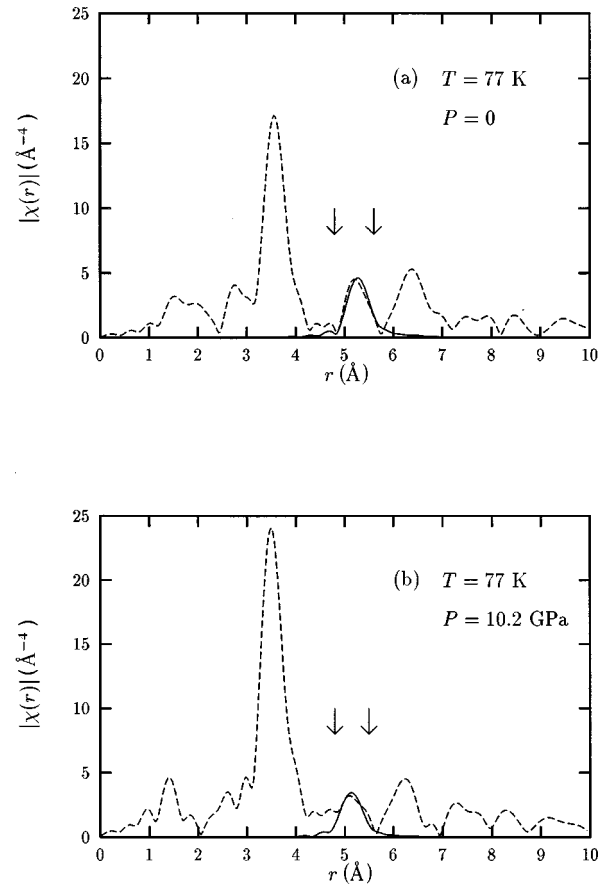


FIG. 6. Fits of calculated Nb-Nb⁽⁵⁾ contributions (solid) to data (dash) at $T=77$ K and (a) ambient pressure and (b) $P=10.2$ GPa. Fitting range is indicated by arrows. Fourier-transform parameters: k range: $5 \text{ \AA}^{-1} < k < 14 \text{ \AA}^{-1}$, weighting factor: k^3 ,

sured at 230 K by neutron diffraction.⁵

It is remarkable that the pressure dependences of the Nb displacements in two macroscopically different structures (rhombohedral at 77 K and orthorhombic at 300 K), follows very closely the same curve (Fig. 8). This supports the view that the local distortions are not sensitive to the the orthorhombic-rhombohedral phase transition. The fact that the short-range order is not significantly affected by the cooperative long-range order effects is further evidence that the Nb displacement from the cubic site is caused predominantly by a short-range interaction.^{3,27}

It is interesting to notice that the effect of pressure on the off-center Nb displacements is much larger than its effect on the lattice constant. For example at room temperature, while

TABLE II. Atomic coordinates $\Delta(\text{O})$, unit cell size a , Nb off-center displacement d at 300 K and different pressures.

P (GPa)	$\Delta(\text{O})$	a , \AA	d , \AA
0	0.0284(8)	4.056(6)	0.200(4)
1.4(4)	0.0263(12)	4.033(9)	0.184(5)
5.3(4)	0.0209(12)	3.996(9)	0.145(4)
8.5(4)	0.0184(17)	3.971(8)	0.127(7)
11.6(4)	0.0162(19)	3.958(7)	0.112(8)
15.8(4)	0.0158(17)	3.931(8)	0.108(7)

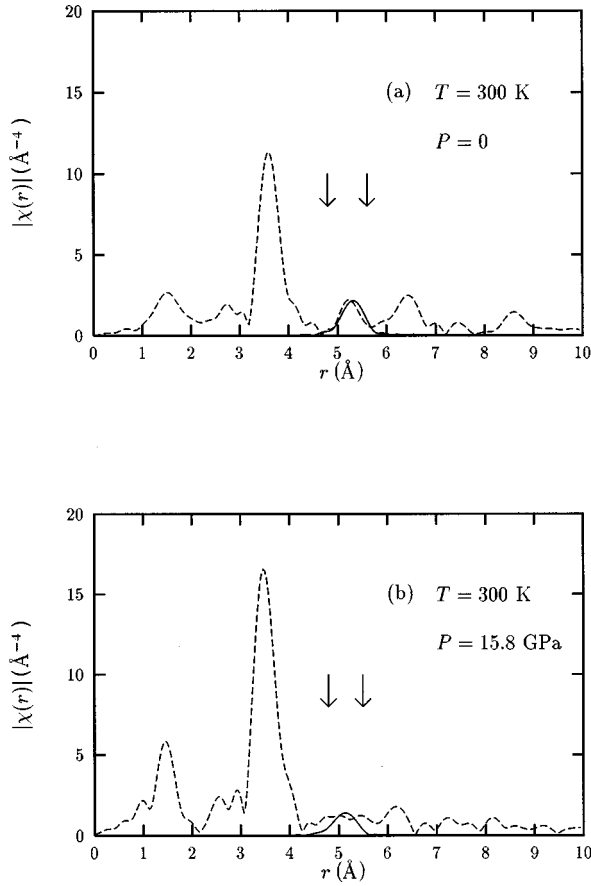


FIG. 7. Fits of calculated Nb-Nb⁽⁵⁾ contributions (solid) to data (dash) at $T = 300$ K and (a) ambient pressure and (b) $P = 15.8$ GPa. Fitting range is indicated by arrows. Fourier-transform parameters: k range: $5 \text{ \AA}^{-1} < k < 14 \text{ \AA}^{-1}$, weighting factor: k^3 ,

the lattice parameter decreases only by 3% within the pressure range investigated, the magnitude of Nb displacements drops gradually by approximately 45% (Table II), from $0.20(1) \text{ \AA}$ to $0.11(1) \text{ \AA}$. This decrease in Nb off-center displacement with pressure is consistent with the progressive decrease in Raman intensity of most TO modes.⁸

The fact that birefringence vanishes and first-order Raman lines vanish or become small above 9 GPa,⁸ suggested that the crystal is cubic above this pressure. In the cubic phase the Nb atom average displacement $d(\text{Nb})$ from the inversion symmetry center must vanish. However, as Fig. 8 demonstrates, $d(\text{Nb})$ changes continuously through the 9 GPa region with no visible slope change. Our results, therefore, confirm the assumption made in Ref. 8 that local distortions may be present in this system well above the suggested phase transition pressure up to at least 18 GPa. However, the distortions are not orthorhombic as Gourdain *et al.*⁸ suggest, but rhombohedral. The difference between XAFS and the

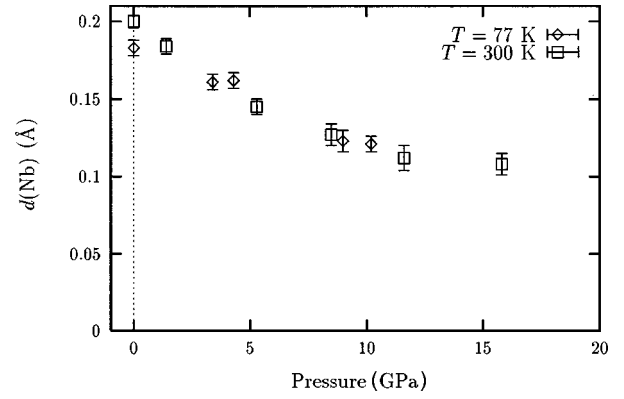


FIG. 8. Change in Nb [111] off-center displacements with pressure at 77 and 300 K.

two optical measurements is explained by their different time scales as discussed in the Introduction, indicating that the local distortions are dynamic and not static.

It is worth noting that the distribution function of the Nb⁽⁰⁾-O⁽¹⁾ distances remains convincingly peaked off the center of the first-neighbor oxygen octahedron along the [111] directions for all pressures since the displacement of the peak persists to be about three times its σ . Because of the good spatial resolution of the XAFS data (0.04 \AA in our case), it is possible to distinguish this off-center distribution from an anisotropic vibration which has a large displacement along the [111] directions but is peaked about the center. Unless the measurement has sufficient spatial resolution it is not possible to make this distinction. For example, this distinction could not be made in measurements of KNbO₃ (Ref. 5) and PbTiO₃ (Ref. 28) using the neutron-diffraction technique.

Mean-square relative deviations of the distances between the Nb⁽⁰⁾ atom and its first, second, fourth, and fifth NN are shown in Fig. 9 for all temperatures and pressures. As Figs. 9(a)–9(c) show, σ^2 of the nearer-neighbor pairs Nb⁽⁰⁾-O⁽¹⁾ and Nb⁽⁰⁾-Nb⁽³⁾ decrease with pressure as expected. As a first approximation, we interpolated the σ^2 -pressure dependence linearly, and used a least-squares method to determine the slope of this dependence. The slopes are tabulated in Table III. σ^2 of the longer Nb⁽⁰⁾-O⁽⁴⁾ and Nb⁽⁰⁾-Nb⁽⁵⁾ pairs, however, have a completely different trend [Figs. 9(d) and 9(e)]. These σ^2 increase with pressure at both temperatures. A similar effect of the increase of the σ^2 of Nb-O (4NN) pair with pressure was observed earlier with XAFS in KNb_{0.87}Ta_{0.13}O₃.¹⁸

The fact that the σ^2 of both Nb⁽⁰⁾-O⁽¹⁾ and Nb⁽⁰⁾-Nb⁽³⁾ decrease with pressure whereas the σ^2 of Nb⁽⁰⁾-O⁽⁴⁾ increases with pressure suggests that the oxygen octahedra librations increase with pressure. We tried unsuccessfully to fit our data assuming ordered octahedra rotations using various rotation

TABLE III. Slope (in $10^3 \text{ \AA}^2/\text{GPa}$) of linearly interpolated change of σ^2 with pressure at 77 and 300 K for Nb-O and Nb-Nb pairs.

T (K)	Nb-O ₁ ⁽¹⁾	Nb-O ₂ ⁽¹⁾	Nb-Nb ⁽³⁾	Nb-O ⁽⁴⁾	Nb-Nb ⁽⁵⁾
77	-0.19(4)	-0.26(6)	-0.09(1)	0.8(4)	0.14(4)
300	-0.19(3)	-0.24(4)	-0.05(1)	0.4(1)	0.27(6)

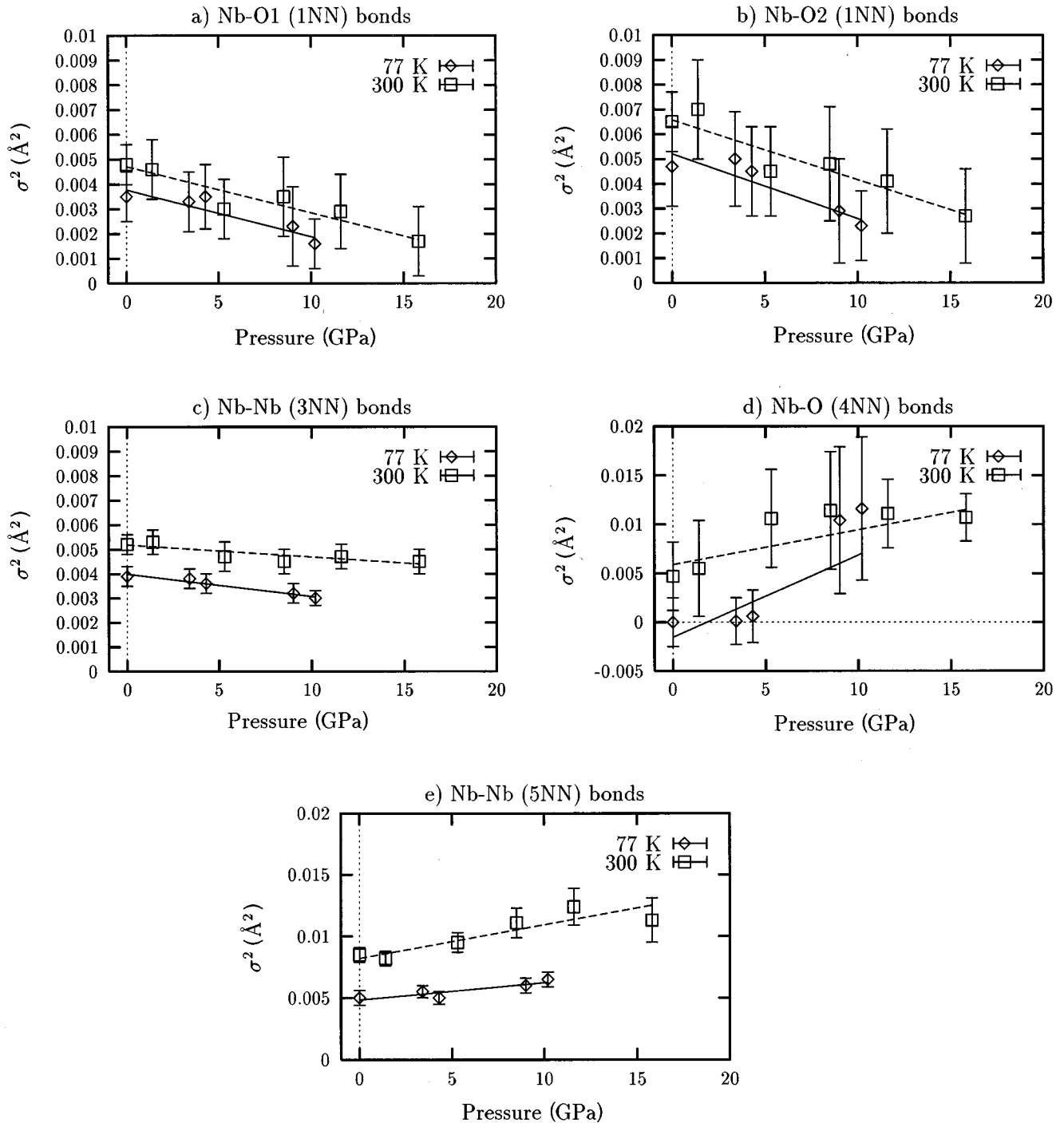


FIG. 9. σ^2 of Nb-O (1NN and 4NN) and Nb-Nb (3NN and 5NN) pair lengths. Straight lines define the slope of linear interpolation (Table III).

axes. The fact that we did not succeed suggests that the rotations are disordered and as previously shown⁴ this means that the octahedra themselves become increasingly distorted with pressure.

The increase in the Nb⁽⁰⁾-Nb⁽⁵⁾ σ^2 with pressure can be explained as follows: the Nb local off-center displacements in the cubic phase are disordered with the Nb atoms displacing along different [111]-type directions in different cells. Comes *et al.*⁶ have shown that at ambient pressure the dis-

placement components along the principle [100]-type axes are highly correlated along these axes. This means that the longitudinal displacements of the Nb probe and its third Nb neighbor are highly correlated along these directions and will yield a small σ^2 . On the other hand, the correlation length for atoms which are not along a [100]-type line is much shorter. This may be the reason that the ambient pressure Nb⁽⁰⁾-Nb⁽⁵⁾ σ^2 (which is not along a [100] direction) is larger than that of Nb⁽⁰⁾-Nb⁽³⁾ (along a [100] direction). The in-

crease in the Nb⁽⁰⁾-Nb⁽⁵⁾σ² with pressure (while that of Nb⁽⁰⁾-Nb⁽³⁾ decreases) suggests that pressure decreases this correlation even further.

VI. SUMMARY AND CONCLUSIONS

Nb *K*-edge XAFS data of KNbO₃ were measured at 77 and 300 K under high pressure. We observed a pressure-induced monotonic displacement of the Nb atom towards the center of oxygen octahedra at both temperatures, 77 and 300 K. The Nb off-center displacements are in the [111]-type directions at all temperatures and pressures measured so far in spite of the fact that the crystal has different crystallographic structures. Moreover, the displacement magnitudes vary in the same way with pressure at both temperatures even though the starting macroscopic structures are different (rhombohedral at 77 and orthorhombic at 300 K).

Our results show that, while the average structure reportedly exhibits one or more pressure-induced phase transitions as observed by room-temperature Raman scattering,^{8,9} the local structure remains rhombohedrally distorted at all pressures up to 15.8 GPa, indicating a significant order-disorder element in the phase transitions.

The increase with pressure of the Nb⁽⁰⁾-O⁽⁴⁾ and the Nb⁽⁰⁾-Nb⁽⁵⁾σ² indicates that pressure increases the oxygen octahedra librations and distortions, and decreases the Nb displacement correlation length. Oxygen perovskites are characterized by a relatively rigid oxygen octahedron. The pressure-induced increased oxygen octahedra librations and distortions may be a precursor of the transition to the amorphous state suggested by Shen *et al.*⁹

ACKNOWLEDGMENTS

This work was supported in part by the University of Washington funds, U.S. DOE grants through the Pacific Northwest National Laboratories, U.S. DOE Grant No. DEFG02-96ER45439 through the Materials Research Laboratory at the University of Illinois at Urbana-Champaign (A.I.F.), U.S. DOE Grant No. DEFG03-97ER45622 (F.M.W., S.K., and R.I.), U.S. DOE Grant No. DEFG06-90ER45425 (D.H. and E.A.S.), and the German-Israeli binational science foundation (Y.Y.). SSRL is supported by the U.S. DOE and National Institutes of Health.

*Present address: Materials Research Laboratory, University of Illinois at Urbana-Champaign. Mailing address: Brookhaven National Laboratory, Bldg. 510 E, Upton, NY 11973.

¹N. Sicron, B. Ravel, Y. Yacoby, E. A. Stern, F. Dogan, and J. J. Rehr *Phys. Rev. B* **50**, 13 168 (1994).

²K. H. Kim, W. T. Elam, and E. F. Skelton, in *Optical Fiber Materials*, edited by J. W. Fleming *et al.*, MRS Symposia Proceedings No. 172 (Materials Research Society, Pittsburgh, 1990), p. 291.

³O. Hanske-Petitpierre, Y. Yacoby, J. Mustre de Leon, E. A. Stern, and J. J. Rehr, *Phys. Rev. B* **44**, 6700 (1991).

⁴B. Rechav, Y. Yacoby, E. A. Stern, J. J. Rehr, and M. Newville, *Phys. Rev. Lett.* **72**, 1352 (1994).

⁵A. W. Hewat, *J. Phys. C* **6**, 2559 (1973).

⁶R. Comes, M. Lambert, and A. Guiner, *Solid State Commun.* **15**, 715 (1974).

⁷Ya. Girshberg and Y. Yacoby, *Solid State Commun.* **103**, 425 (1997).

⁸D. Gourdain, E. Moya, J. C. Chervin, B. Canny, and Ph. Pruzan, *Phys. Rev. B* **52**, 3108 (1995).

⁹Z. X. Shen, Z. P. Hu, T. C. Chong, C. Y. Beh, S. H. Tang, and M. H. Kuok, *Phys. Rev. B* **52**, 3976 (1995).

¹⁰R. Ingalls, E. D. Crozier, J. E. Whitmore, A. J. Seary, and J. M. Tranquada, *J. Appl. Phys.* **51**, 3158 (1980).

¹¹K.-Q. Lu and E. A. Stern, *Nucl. Instrum. Methods Phys. Res.* **212**, 475 (1983); E. A. Stern and K. Kim, *Phys. Rev. B* **23**, 3781 (1981).

¹²E. A. Stern, M. Newville, B. Ravel, Y. Yacoby, and D. Haskel, *Physica B* **208&209**, 117 (1995). The UWXAFS analysis package has been licensed by the University of Washington. Information concerning acquiring the package can be obtained by e-mail to

stern@u.washington.edu, or at the WWW URL <http://krazy.phys.washington.edu>.

¹³M. Newville, P. Livins, Y. Yacoby, J. J. Rehr, and E. A. Stern, *Phys. Rev. B* **47**, 14 126 (1993).

¹⁴E. A. Stern and S. M. Heald, in *Handbook on Synchrotron Radiation*, edited by E. E. Koch (North-Holland, New York, 1983), Vol. 1.

¹⁵S. I. Zabinsky, J. J. Rehr, A. Ankudinov, R. C. Albers, and M. J. Eller, *Phys. Rev. B* **52**, 2995 (1995).

¹⁶*American Institute of Physics Handbook*, 3rd ed., edited by D. E. Grey (McGraw-Hill, New York, 1972).

¹⁷M. Delannoy-Coutiris and C. Perrin, *Mech. Mater.* **12**, 25 (1991).

¹⁸F. Wang, B. Ravel, Y. Yacoby, E. A. Stern, and R. Ingalls, *J. Phys. IV* **7**, C2-1225 (1997).

¹⁹B. Ravel and E. A. Stern, *Physica B* **208&209**, 316 (1995).

²⁰E. A. Stern, *Phys. Rev. B* **48**, 9825 (1993).

²¹P. A. Lee and J. B. Pendry, *Phys. Rev. B* **11**, 2795 (1975).

²²B.-K. Teo, *J. Am. Chem. Soc.* **103**, 3990 (1981).

²³A. Frenkel, E. A. Stern, A. Voronel, M. Qian, and M. Newville, *Phys. Rev. B* **49**, 11 662 (1994).

²⁴A. Frenkel, E. A. Stern, M. Qian, and M. Newville, *Phys. Rev. B* **48**, 12 449 (1993).

²⁵D. C. Koningsberger (private communication).

²⁶D. Haskel, B. Ravel, M. Newville, and E. A. Stern, *Physica B* **208&209**, 151 (1995).

²⁷E. A. Stern and Y. Yacoby, *J. Phys. Chem. Solids* **57**, 1449 (1996).

²⁸R. J. Nelmes and W. F. Kuhs, *Solid State Commun.* **54**, 721 (1980); R. J. Nelmes, R. O. Piltz, W. F. Kuhs, Z. Tun, and R. Restori, *Ferroelectrics* **108**, 165 (1990).